

# Rapid and Semi-analytical Design and Simulation of a Toroidal Magnet Made With YBCO and MgB<sub>2</sub> Superconductors

I K Dimitrov<sup>1,2</sup>, X Zhang<sup>1</sup>, V F Solovyov<sup>1</sup>, O Chubar<sup>3</sup> and Qiang Li<sup>1</sup>

<sup>1</sup> Condensed Matter Physics and Materials Science Department, Brookhaven National Laboratory, Upton, New York 11973, USA

<sup>2</sup> System Evaluation Division, Institute for Defense Analyses, 4850 Mark Center Drive, Alexandria, VA 22311, USA

<sup>3</sup> Photon Sciences Directorate, Brookhaven National Laboratory, Upton, New York 11973, USA

E-mail: [idimitrov@bnl.gov](mailto:idimitrov@bnl.gov)

PACS numbers: 88.80.fj, 84.60.Ve, 84.71.Ba, 85.25.-j

*Keywords:* energy storage, superconductivity, SMES, 2G YBCO tape, MgB<sub>2</sub> wire

**Abstract.** Recent advances in second generation (YBCO) high temperature superconducting wire could potentially enable the design of super high performance energy storage devices that combine the high energy density of chemical storage with the high power of superconducting magnetic storage. However, the high aspect ratio and considerable filament size of these wires requires the concomitant development of dedicated optimization methods that account for the critical current density in type II superconductors. Here, we report on the novel application and results of a CPU-efficient semi-analytical computer code based on the *Radia* 3D magnetostatics software package. Our algorithm is used to simulate and optimize the energy density of a superconducting magnetic energy storage device model, based on design constraints, such as overall size and number of coils. The rapid performance of the code is pivoted on analytical calculations of the magnetic field based on an efficient implementation of the Biot-Savart law for a large variety of 3D "base" geometries in the *Radia* package. The significantly-reduced CPU time and simple data input in conjunction with the consideration of realistic input variables, such as material-specific, temperature and magnetic field-dependent critical current densities have enabled the *Radia*-based algorithm to outperform finite element approaches in CPU time at the same accuracy levels. Comparative simulations of MgB<sub>2</sub> and YBCO-based devices are performed at 4.2 K, in order to ascertain the realistic efficiency of the design configurations.

## 1. Introduction

Superconducting magnetic energy storage (SMES) has been traditionally considered for power conditioning applications, where instantaneous high power can be delivered in a matter of milliseconds. Among the advantages exclusively offered by superconductors we could mention: *i*) higher energy storage efficiency ( $\sim 95\%$ ) than other existing energy storage systems [1], and *ii*) almost-immediate charge/discharge characteristics [2, 3]. Currently, SMES is one of a few applications that is adaptable to the needs of the electric utilities markets [4].

Recently, a renewed interest in SMES technologies has been motivated by the search for means of improving the stability of the future power grid system, that would incorporate a large number of intermittent energy sources, such as wind and solar [5, 6, 7]. Low-temperature superconductors, such as

Nb-Ti, have been successfully used for SMES, however, issues with reliability of 4.2 K cryogenics, efficiency of power electronics, and the relatively low energy density of Nb-based SMES have limited the applicability of the technology to a few cases, where electric power quality is at premium [8, 9, 10].

So far, second generation (2G) high temperature superconductor (HTS)  $\text{YBa}_2\text{Cu}_3\text{O}_7$  (YBCO) has offered the greatest hope for implementation, since it exhibits all-around superior properties to all other classes of superconductors [11], especially in light of the fact that it offers a possibility of operation at a temperature much higher than that of liquid helium [12]. However, other promising candidates have emerged throughout the years as well, such as magnesium diboride,  $\text{MgB}_2$  [13] and the recently-discovered iron-based superconductors [14].

Magnet design has become a process of paramount importance to SMES performance, necessitating better and faster analytical tools, since magnetic field calculations in and around a SMES demand sizeable CPU time and memory. The Finite Element Method (FEM) has been the most common tool currently utilized for computations of magnetic fields in superconducting magnetic energy storage devices.

In this report, we present an alternative approach towards building an algorithmic solution for simulating and optimizing a SMES device based on a selection of superconducting materials, such as second-generation YBCO tape or  $\text{MgB}_2$ . This method is based on the *Radia* software package, which is written in object-oriented C++, and interfaced to Mathematica via MathLink. A substantial portion of algorithmic processing in the scope of this work is implemented in the Mathematica language. Here, *Radia* is used to assess the fields created by 3D volumes with constant current density, based on the Biot-Savart law.

## 2. Methodology

### 2.1. Geometrical Considerations

Generally, there exist several types of geometrical arrangements for building a SMES [1, 15, 16], but the toroidal design offers the advantage of a reduced stray (perpendicular) magnetic field on the tape or wire, mostly confining the field inside the coil. Such an arrangement is especially critical for second generation (2G) YBCO tape, since YBCO is marked by a high critical current density anisotropy,  $\gamma_m$ . In the case of YBCO, the in-plane  $J_c^{\parallel ab}(B = 17 \text{ T}) = 10.8 \text{ MA/cm}^2$ , for example, can exceed the out of plane one  $J_c^{\perp ab}(B = 17 \text{ T}) = 1.8 \text{ MA/cm}^2$  by roughly an order of magnitude at 4.2 K.

### 2.2. The Radia Software and Its Applications

The SMES simulation reported here has been built on top of the *Radia* software package using *Mathematica* by Wolfram Research [17]. The *Radia* software package was designed by scientists at the European Synchrotron Radiation Facility (ESRF), for solving physical and technical problems one encounters during the development of insertion devices for synchrotron light sources. However, it can also be used in different branches of physics, where efficient solutions of 3D boundary problems of magnetostatics are needed [17, 18].

Creating and linking the objects properly is the first step in describing the magnetostatics problem. Contrary to the FEM approach, *Radia* does not mesh the vacuum (an example of a FEM geometrical segmentation and field generation is shown in Fig. 1) [18], but rather, solves boundary magnetostatic problems with magnetized and current-carrying volumes, using the boundary integral approach. The current-carrying elements can be straight or curved blocks [19], and the planar boundary conditions are simulated via sets of space transformations, such as translations, rotations, or plane symmetry inversions [19]. Applying transformations with a multiplicity can be understood as an efficient use of the symmetries

in the model being solved. This results in a minimum number of degrees of freedom, and therefore, dramatically reduces the memory requirements and CPU time needed to obtain a solution [17].

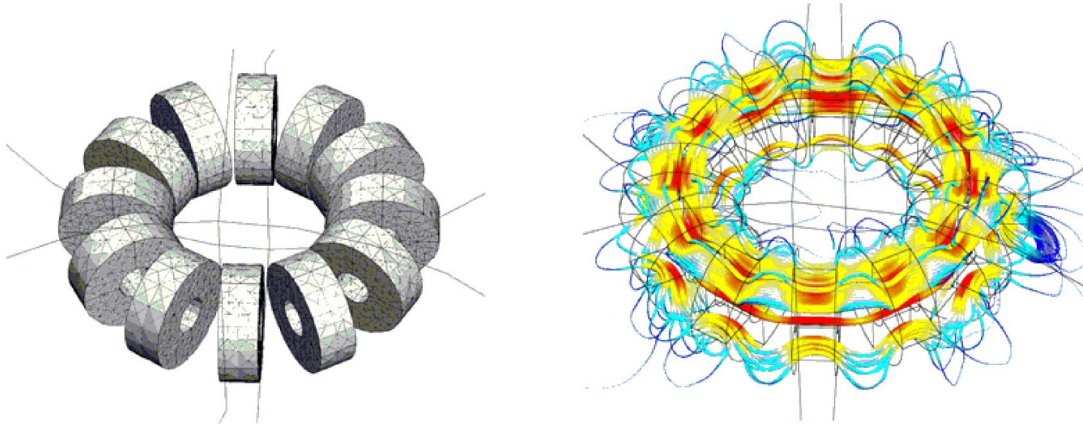


Figure 1: A typical Finite Element Methods simulation of a SMES via COMSOL. A simulation of the geometric dimensions and arrangement of the coils is shown on the left, whereas the resulting magnetic field distributions derived from a particular electrical current density are shown, juxtaposed onto the coil geometry, is shown on the right.

The reduction of the necessary elements for precisions comparable to FEM approaches (see Fig. 2) [20, 21] leads to a drastic reduction of the required CPU time. This time efficiency is crucial when it comes to creating SMES optimization algorithms.

In the current work, we employed *Radia* to simulate and optimize a realistic SMES device, which takes into account the temperature and magnetic field dependent critical current density,  $J_c(T, B)$ , of the superconducting wire of choice used in the simulation (second generation YBCO tape or MgB<sub>2</sub>).

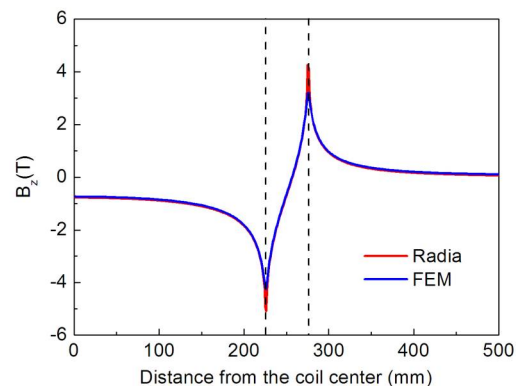


Figure 2: Typical distribution of the magnetic field inside a superconducting coil calculated by *i*) FEM (in blue), and *ii*) *Radia* (in red). One of the issues with *Radia* is the emergence of singularities at boundaries, as seen in the figure. The two field profiles overlap everywhere except at the coil boundary, where *Radia* unphysically diverges (due to the analytical approximation used).

### 2.3. Computational Procedure

Our algorithm starts by specifying the actual geometry of the device, which is built according to given specifications, such as *i*) coil radius, *ii*) coil thickness, *iii*) coil width, *iv*) coil thickness, *v*) toroidal radius, and *vi*) number of coils. The coil radius is defined as the mean of the inner and outer radii (with respect to the coil's axis of symmetry) of each coil, while the coil thickness is the difference between these two (see Fig. 3). The large (toroidal) radius is the distance from the geometric center of the SMES to the geometric center of each individual coil, and the typical toroidal radii that we employed were on the order of 1 – 2 meters.

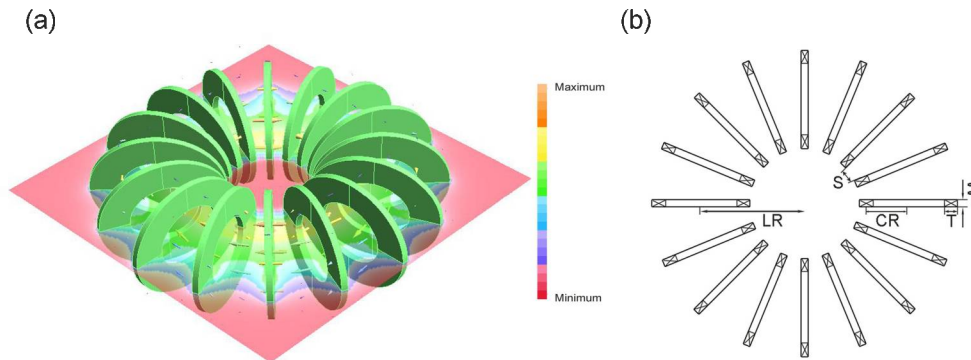


Figure 3: (a) Structural concept of a 16-module toroidal system generated by *Radia*, with (b) design variables. *LR*, *CR* and *W* stand for the toroidal ("long") radius, coil radius and width, respectively.

*Radia* gives the freedom of choosing the degree of segmentation of each coil; the more segments are chosen, the closer the geometry is to an ideal cylindrical shape, but it will also result in longer computation time. We "built" coils with 50 segments for the actual simulations.

In order to test the validity of *Radia*-based simulations, we compared the outputs of our *Radia*-generated SMES design with that of a FEM simulation by Lee *et al.* [22]. We computed the maximum magnetic fields parallel and perpendicular to the test coil, as well as the total energy stored in the device using the same geometry and operating current density as used by Lee *et al.*, and observed a discrepancy of less than 1% between the two methods. The comparison between the two approaches is shown in Table 1.

Table 1: Comparison of *Radia* and FEM-generated 2.5 MJ toroidal SMES configuration.

Specification	In this work	From Lee <i>et al.</i> [22]
Operating Current Density (A/mm <sup>2</sup> )	194.5	194.5
Max parallel magnetic field (T)	8.8	8.1
Max perpendicular magnetic field (T)	1.12	1.16
Stored Energy (MJ)	2.6	2.6
Total length of HTS conductor (km)	19.58	19.55

### 2.4. Magnetic Field Distribution Computation

The highest field limits the maximum critical current density  $J_c$ .

We present magnetic field analysis results of a toroidal-type SMES magnet calculated via *Radia* (see Fig. 4). A characteristic magnetic flux density pattern of the center plane of the toroid is exhibited in Fig. 4a, while typical perpendicular,  $B_N(x)$ , and tangential,  $B_T(x)$ , flux density profiles along the radial direction of a single pancake coil are shown in Fig. 4b. For this particular simulation the operating current of the magnet is taken to be 960 A, while the maximum perpendicular magnetic flux density, tangential magnetic flux density and stored energy of the simulated device obtained from the simulation are shown to be 1.01 T, 9.00 T and 2.68 MJ, respectively. The discrepancies between the maxima of the *i*) perpendicular magnetic flux density, and *ii*) tangential magnetic flux density, obtained via FEM and *Radia* were shown to be on the order of 2%.

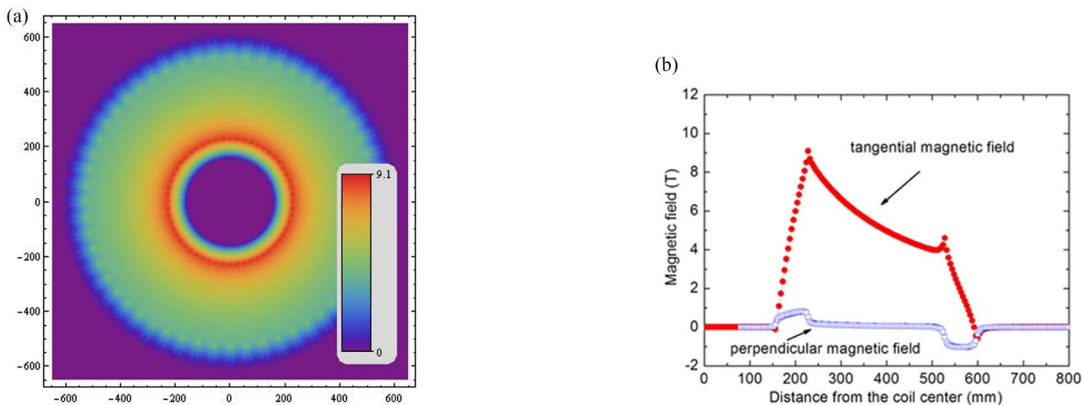


Figure 4: (a) Magnetic flux density pattern of the center plane of toroidal-type SMES magnet; (b) Shown are the *i*) perpendicular and *ii*) tangential flux density analyses on a typical single pancake coil, in open gray and filled red circles, respectively.

One of the conclusions one can immediately draw from the analysis of the field distribution, as evidenced in Fig. 4a, is that the field is mostly confined inside the coil. Being able to confine the magnetic field inside the coil is important for a number of reasons: *i*) large field gradients could be avoided from the coil edges (thus affecting the  $J_c(B)$  of the wire), and *ii*) stray fields are generally detrimental to electronic devices located in the vicinity of the magnet. Thus, SMES designs with large numbers of coils may be preferred for as long as geometrical and critical current limitations are considered and met [23].

Not surprisingly, the highest  $B_T$ 's are found at the inner rim of an individual coil, nearest the center of the torus along the  $z = 0$  plane, as evidenced in Fig. 4, *i.e.*,  $B_T$  does not exhibit a  $y$ -axis mirror symmetry through the center of the coil, which is clearly due to the higher density of current-carrying elements closer to the torus center. On the other hand,  $B_N$  is shown to be several times smaller than  $B_T$ .  $B_N$  is supposed to vanish in the case of a perfect toroidal SMES with a continuum of coils. However, there is always a finite  $B_N$  for a SMES magnet built up with a discrete number of coils. It should be noted that although  $B_N$  is several times smaller than  $B_T$ , YBCO tapes are marked by a large anisotropy in the critical current density ( $J_c(B_N) \ll J_c(B_T)$ ), and therefore the maximum  $B_N$  determines the current density cutoff that ought to be compared against the  $J_c(B)$  used in SMES design.

### 3. SMES Design

#### 3.1. Optimization Algorithm Overall Flow

Once the SMES geometry is specified, we feed the critical current density curves for *i*) MgB<sub>2</sub> and *ii*) 2G YBCO tape for different temperatures and field ranges into the code. Subsequently, the magnetic field is

scanned inside the coil and the maximal  $B$ ,  $B_{max}$ , is utilized in the calculation of the minimal  $J_c^{min}$ , which would serve as the SMES design bottleneck. The ratio of a trial value of the current density,  $J(B)$ , to  $J_c^{min}(b)$  [24], is an indicator of the stability of the system, and is known as the "load factor". Depending on the value of the load factor, our algorithm chooses whether the thickness ought to increase or decrease in order for the requirement to be met. Our load factor is set at 70% of  $J_c^{min}$ , so if  $J > 0.7 \cdot J_c^{min}$ , the algorithm increases the coil thickness and reduces  $J$  by a proportionate amount since the total energy is proportional to the square of the current. Analogously, if  $J < 0.7 \cdot J_c^{min}$ , the code "removes" turns (and proportionately increases  $I$ ), until  $J = 0.7 \cdot J_c^{min}$ . The design flow of the entire optimization process is shown in Fig. 5

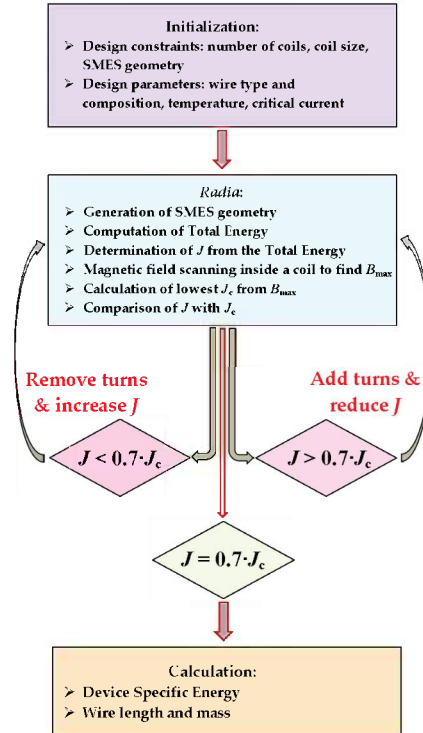


Figure 5: Design process flow of SMES simulation and optimization routine. The consecutive iteration generates the device specific energy (total stored energy / total wire mass) in  $CR - W$  space.

Once the SMES configuration is optimized, the algorithm performs the same operation as a function of *i*) Coil Radius ( $CR$ ) and *ii*) Coil Width ( $W$ ).  $CR$  is a continuous variable for the purposes of the simulation, and therefore it could be varied in steps of arbitrary size. On the other hand,  $W$  is a multiple of either the diameter of the wire (in the case of  $MgB_2$ , or the width of the tape (in the case of 2G wire). Then, *i*) the total energy,  $E_T$ , of the optimized configuration is computed, and *ii*)  $E_T$  is divided by the total wire mass of the SMES, resulting in the device specific energy,  $\rho_E$ .

### 3.2. Assessing $B_{max}$

There are a number of prospective SMES applications which require stored energies  $\sim 10^7 - 10^9$  J, and most of our efforts have been focused predominantly on that energy range, particularly when considering

overall dimensions on the 1 – 2 meter scale. The dimensional considerations of such a device are very important, especially if it is to be transportable and/or integrated with other technological instruments.

In order to devise the algorithm that assesses the maximal internal magnetic field, we consider two  $10^7$  Joule SMES design cases at 4.2 K: *i*) a SMES built of  $\text{MgB}_2$  wire, and *ii*) a SMES built of 2G tape, both of which contain 20 turns, Long Radius,  $LR, = 1000$  mm, coil radius,  $CR, = 200$  mm, coil width,  $W, = 96$  mm, coil thickness,  $T, = 100$  mm. Then, we scan the magnetic field of the  $\text{MgB}_2$  SMES coil transversely, going through the middle of the coil and assessing the absolute value of  $B$  in the  $\text{MgB}_2$  case, where the field is expected to be the highest (see Inset of Fig. 6a). In the case of 2G wire, we scan along the edge of the coil, as shown in the Inset of Fig. 6b, and assess only the perpendicular  $B$  component, since this is the application bottleneck, as discussed in Section 2.5.

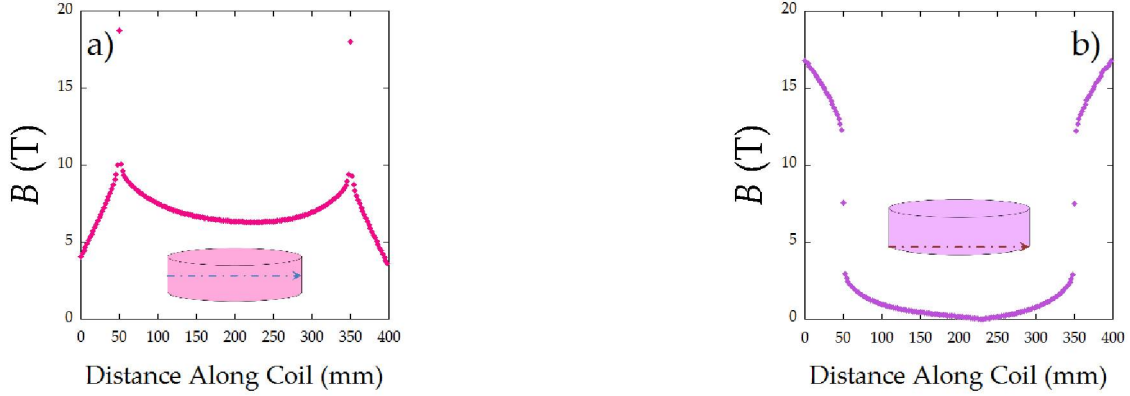


Figure 6: Transverse magnetic field scans through a)  $\text{MgB}_2$  and b) YBCO SMES coils. The directions of scanning are shown in the insets of each figure. The highest total  $B$  fields are expected in the middle of a coil, and thus we scan across the middle of the coil for  $\text{MgB}_2$ . However, in the case of YBCO, only  $B_N$  is assessed (see Section 2.5), along the edge, where the field "leaks out" between the coils and thus, the highest  $B_N$  is expected. Note the singular points at 50 mm and 350 mm from the inner edge of the coil – a *Radia* artifact, which need to be removed from the analysis.

As one can see from Fig. 6a, *Radia* tends to produce an unphysical singularity in the vicinity of  $B_{max}$ , as evidenced in the points at 50 mm and 350 mm from the inner edge of the coil at the stored energy used in the simulation. Choosing any of these two points ("artifacts" on the conductor boundary) could lead to erroneous  $J_c(B)$  results. The excessively high field at the conductor boundary does not disappear as we change the level of segmentation of each coil. *Radia* assumes a constant  $J_c$  over the entire coil and does not perform any "relaxation" with respect to the current density/field in different areas of the conductor, suggesting this could lead to an excessively high field at the edge, and pointing to an area of future improvement. Thus, instead of picking the maximal point from the scan, we identify its location, and fit the data points on either side of the singularity with a tenth order polynomial and get the mean of the two functions at the intersection (maximal point) location. We get  $B_{max} = 10.68$  T using this algorithm, which is consistent with the cusp at 50 mm from the inner edge of the coil. This procedure has led to smooth analytic energy density surfaces.

Analogously, in order to avoid any *Radia*-generated artifacts, we have imposed a 90% cutoff from the scanned  $B_{max}$  in the YBCO case, *i.e.*, only field values  $\leq 90\%$  of  $B_{max}$  are considered. The truncated data is subsequently fitted with a tenth order polynomial and the maximal value is extracted from this fit.

The resulting  $B_{max}$  were used to calculate the (lowest) critical current densities found in a single SMES coil for a given geometry and energy storage requirement, as outlined in the previous subsection. Every

time an input parameter changes, the code would scan for  $B_{max}$  *de novo*.

### 3.3. Wires, Tapes and their $J_c$ 's

Upon designing the SMES geometry based on a given toroidal radius and coil dimensions [25], we specify the wire characteristics of two different conductors: *i*) a  $\text{MgB}_2$  wire which we assume in our calculation is a monofilamentary strand of  $\text{MgB}_2$ , as discussed by Li *et al.* [26, 27] and *ii*) standard second generation (2G) [28, 29, 30, 31]. The rapid advances in applied superconductivity, such as the successful implementation of pulsed-laser deposition techniques to grow iron-chalcogenide superconducting film on metal substrates [11, 32, 33, 34, 35, 36, 37] will hopefully lead to the development of commercial Fe-based superconducting wire in the near future, as well.

The  $J_c(B)$  data utilized in the simulation can be found in References [26], [38], and [39].

Analytical fits of double-bending functions were used to obtain functional forms for  $J_c$ 's at different temperatures for both 2G YBCO and  $\text{MgB}_2$  wires. In principle, double-bending functions have been shown to be very effective in fitting the front and tail ends of  $J_c(B)$ , as if the two data curvatures are distinguishable [40]. However, being able to discern between two functional forms needed for a fit would require a much greater density of  $J_c(B)$  data points, which would be a necessary requirement for a realistic SMES engineering.

## 4. Results and Discussion

Simulations were run for both 2G tape and  $\text{MgB}_2$  wire at 4.2 K. In the case of the (2G) YBCO device the simulation was run for a SMES comprising 20 coils, initial coil radius,  $CR_0 = 400$  mm, initial coil width,  $W_0 = 96$  mm, initial coil thickness,  $T_0 = 100$  mm, and constant  $LR = 1500$  mm. In the case of the  $\text{MgB}_2$  wire-based SMES 32 coils were considered, along with  $CR_0 = 400$ ,  $W_0 = 96$  mm,  $T_0 = 100$  mm and  $LR = 2000$  mm. For both simulations the number of segments was chosen to be 50, and the number of points considered in the configuration space of the project (the  $CR - W$  plane) was fixed at 1,500 [41].

Both sets of devices were simulated under the initial provision that they would store  $10^8$  Joules of energy [42]. The optimization was performed at every point in the specified segment of  $CR - W$  space, and the *i*) energy, *ii*) device specific energy, *iii*)  $T$ , *iv*)  $CR$ , *v*)  $W$ , *vi*) total SMES mass,  $M$ , and *vii*) total wire length needed,  $L$ , were assessed at each of the 1,500 points (see Fig. 7).

For higher values of  $CR$  and  $W$ , the value of the total energy is actually closer to  $10^9$  J, most likely due to non-linear effects as one can expect a geometric change to bring about. Larger coils, in radius and width, would have coils in a closer proximity to one another (we never change the values of the  $LR$ 's once fixed in the beginning), suggesting that fewer field lines will "leak" in the spaces between them, improving on the overall efficiency of the device. The reason why we could not extend the simulation for arbitrarily large  $CR$ 's and  $W$ 's had to do with the unphysical overlap of coils that our optimization would bring about.

The values of several SMES parameters were obtained at the highest device specific energies from our  $CR - W$  configuration space (see Table 2), and from the comparison between the simulations of the 2G YBCO and  $\text{MgB}_2$  based SMES devices, we notice that while the overall dimensions and stored energies are very comparable, a YBCO-based SMES weighs less than half of its  $\text{MgB}_2$  counterpart. Also, the YBCO device has more than double the device specific energy compared to the one made of  $\text{MgB}_2$  wire at the present energy-storage capacity.

After optimizing every point in configuration space, we were able to get an estimate of the overall length of wire needed (see Fig. 8). One thing to notice is that the  $\text{MgB}_2$ -based device would require 2–3

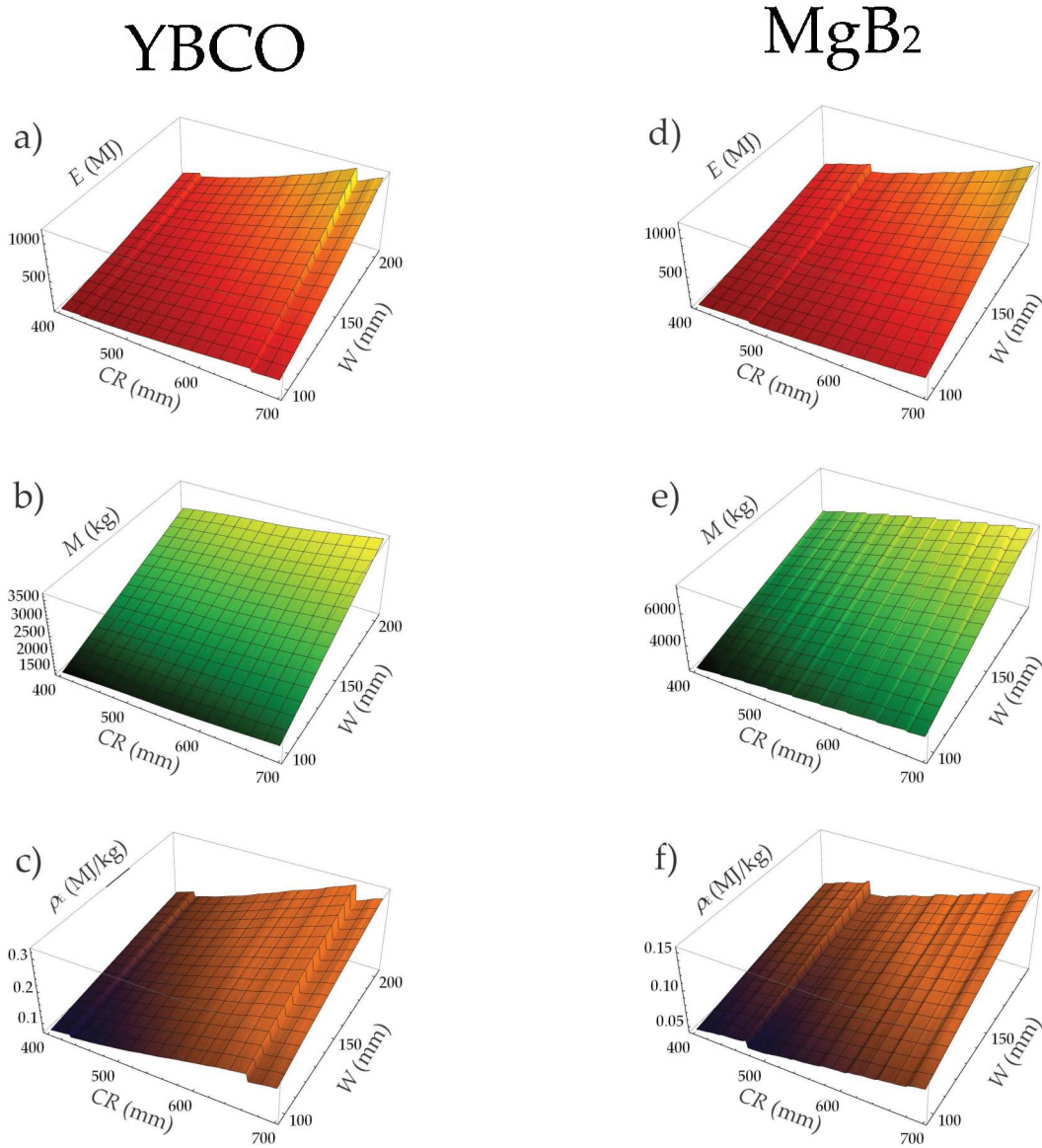


Figure 7: Shown are the outputs of the simulation: a) total energy stored, b) total wire mass, and c) device specific energy in the YBCO 2G SMES. The corresponding d) total energy stored, e) total wire mass, and f) device specific energy for MgB<sub>2</sub> are shown in juxtaposition. The "ripples" observed in the various quantities are artifacts of the simulation (see text).

Table 2: Comparison of design parameters for 20-coil YBCO and 32-coil MgB<sub>2</sub>-based SMES devices at maximum device specific energy.

SMES Type	$\rho_E^{max}$ (MJ/kg)	$M^{max}$ (kg)	$E_{Total}^{max}$ (MJ)	$CR^{max}$ (mm)	$W^{max}$ (mm)	$T^{max}$ (mm)
YBCO	0.327	3,416	1,117.07	662	204	68.7
MgB <sub>2</sub>	0.155	7,537	1,168.26	698	196.8	50.3

fold more wire, in absolute length, for comparable amount of stored energy when compared to its YBCO counterpart (see Table 3).

Table 3: Comparison of wire length requirements (in kilometers) for 20-coil YBCO and 32-coil MgB<sub>2</sub>-based SMES devices at *i*)  $CR = 400$  mm,  $W = 100$  mm and *ii*)  $L(CR = 700$  mm,  $W = 200$  mm.

SMES Type	$L(CR = 400 \text{ mm}, W = 100 \text{ mm})(\text{km})$	$L(CR = 700 \text{ mm}, W = 200 \text{ mm}) (\text{km})$
YBCO	130	341
MgB <sub>2</sub>	332	1,018

## 5. Conclusions

In this paper we demonstrated the viability of *Radia* as a CPU-efficient semi-analytical method for optimizing prospective SMES devices. By altering various device parameters, such as coil radii and thicknesses, we were able to calculate the optimal coil dimensions and simulate total stored energies in YBCO and MgB<sub>2</sub>-based devices. The second generation device exhibits at least a two-fold higher device specific energy compared to the MgB<sub>2</sub> one in the  $10^7$ – $10^9$  J range at 4.2 K. Subsequently, whenever dimensional considerations are critical, YBCO wire will likely be the material of choice. However, if dimensional or weight considerations could be subordinated for the benefit of cost, then the unit price of the wire will be the determining factor.

The value of developing speedy optimization algorithms for SMES stretches beyond the quest for

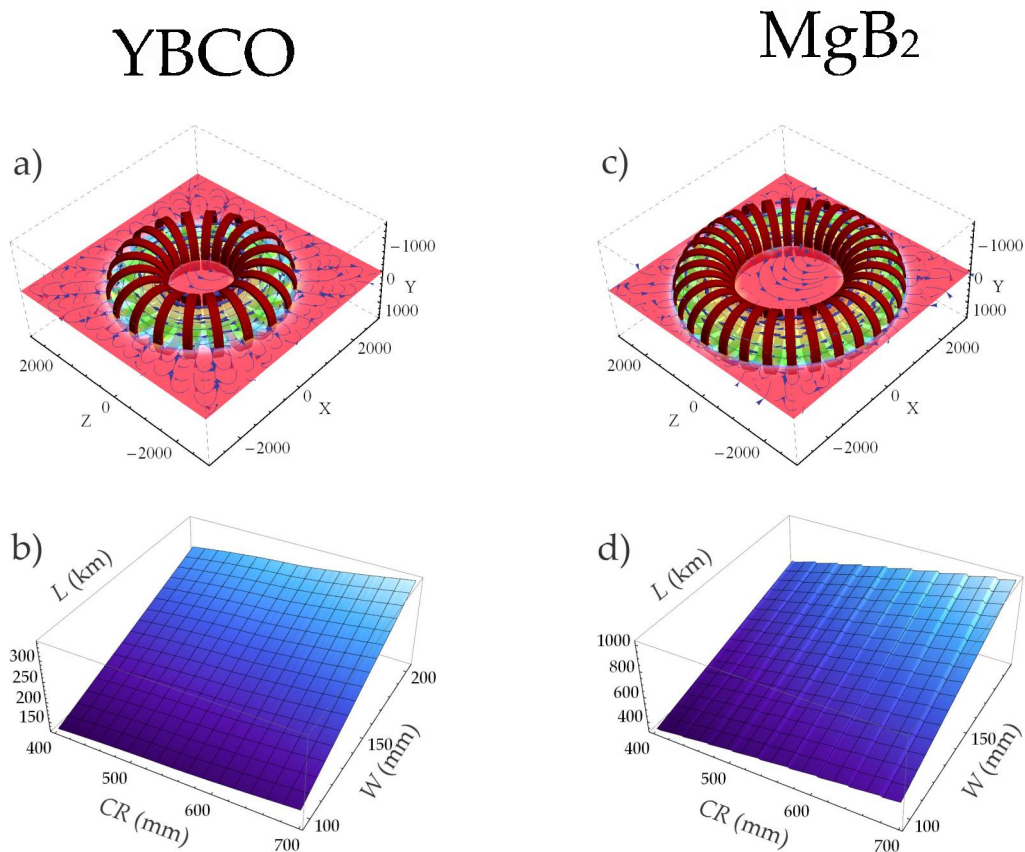


Figure 8: Shown are the final configuration outputs at maximum energy density for a) YBCO and b) MgB<sub>2</sub> devices. All the dimensions in a) and c) are given in millimeters. The total wire length requirements for each optimized configuration in  $CR - W$  are shown for YBCO and MgB<sub>2</sub>-based devices in b) and d), respectively.

efficient and reliable energy storage and rapid release. Moreover, in addition to power storage, there exist certain niche applications which necessitate the integration of a SMES into a propulsion mechanism. An example of such a hybrid would be a superconducting self-supplied electromagnetic launcher (S<sup>3</sup>EL) [2], where the optimum geometry needed to ensure that the magnetic flux from the SMES goes between the launcher rails may be potentially dipole-like, rather than being solenoidal or toroidal [2]. However, the low inductance values needed for typical applications may disfavor the former in favor of the latter two [2]. Thus, the rapid assessment of optimal geometry for a S<sup>3</sup>EL [43] is another prospective employment of *Radia*-based modeling that possesses the potential of becoming industry-enabling.

## 6. Acknowledgements

This work was primarily supported by the US Department of Energy, Office of Basic Energy Science, Materials Sciences and Engineering Division, under contract no. DEAC0298CH10886. Additional support from Air Force Research Lab (V.F.S. and I.K.D.) and NYSERDA (V.F.S.) are also acknowledged. This effort was also supported by the System Evaluation Division of the Institute for Defense Analyses. I.K.D. wishes to thank Steve Warner for interest taken in the current work as well as for critical reading of the manuscript, and Michael Ambroso for technical assistance.

## References

- [1] K. Y. C. Cheung, S. T. H. Cheung, R. G. Navin De Silvia, M. P. T. Juvonen, R. Singh, J. J. Woo *Large-Scale Energy Storage Systems*, Imperial College, London (2002/2003).
- [2] Arnaud Badel, Pascal Tixador, and Michel Arriet, *Supercond. Sci. Technol.* **25**, 014006 (2010) and references therein.
- [3] M. H. Ali, B. Wu, R. A. Douglas, *IEEE Trans. Sustain. Energy* **1**, 38 – 46 (2011).
- [4] W. Buckles and W.V. Hassenzahl, "Superconducting magnetic energy storage" *Power Engineering Review*, *IEEE* **20** (5), p. 16 – 20 (2000).
- [5] H. J. Kim, K. C. Seong, J. W. Cho, J. H. Bae, K. D. Sim, S. Kim, E. Y. Lee, K. Ryu, and S. H. Kim, *IEEE Trans. Appl. Supercond.* **16**, 574 (2006).
- [6] Xiaohua Jiang, Xiaoguang Zhu, Zhiguang Cheng, Xiaopeng Ren, and Yeye He, *IEEE Trans. Appl. Supercond.* **15**, 1903 (2005).
- [7] R. Mikkonen, T. Kalliohara, A. Korpela, J. Lehtonen, R. Perala, *Supercond. Sci. Technol.* **16**, 946 (2003).
- [8] Xianrui Huang, Stephen F. Kral, Gregory A. Lehmann, Yury M. Lvovsky and Minfeng Xu, *IEEE Trans. Appl. Supercond.* **5**, 428 (1995).
- [9] Xianrui Huang, *IEEE Trans. Appl. Supercond.* **5**, 354 (1995).
- [10] J. D. Rogers, H. J. Boenig, J. C. Bronson, D. B. Colyer, W. V. Hassenzahl, R. D. Turner, and R. I. Schermer, *IEEE Trans. Magn.* **15**, 820 (1979).
- [11] Qiang Li, Weidong Si, and Ivo K. Dimitrov, *Rep. Prog. Phys.* **74**, 124510 (2011), and references therein.
- [12] David Larbalestier, Alex Gurevich, D. Matthew Feldmann and Anatoly Polyanskii, *Nature* **414**, 368 (2001).
- [13] Jun Nagamatsu, Norimasa Nakagawa, Takahiro Muranaka, Yuji Zenitani, and Jun Akimitsu, *Nature* **410**, 63 (2001).
- [14] Y. Kamihara, T. Watanabe, M. Hirano, and H. Hosono, *J. Am. Chem. Soc.* **130**, 3296 (2008).
- [15] [http://en.wikipedia.org/wiki/Superconducting\\_magnetic\\_energy\\_storage](http://en.wikipedia.org/wiki/Superconducting_magnetic_energy_storage).
- [16] Myung-Jin Park, Sang-Yeop Kwak, Woo-Seok Kim, Seung-Wook Lee, Ji-Kwang Lee, Kyeong-Dal Choi, Hyun-Kyo Jung, Ki-Chul Seong, and Song-yop Hahn, *Cryogenics* **47**, 391-396 (2007).
- [17] P. Elleaume, O. Chubar, and J. Chavanne, *Proceedings of the 1997 Particle Accelerator Conference* **1–3**, 3509-3511 (1997).
- [18] <http://www.esrf.eu/Accelerators/Groups/InsertionDevices/Software/Radia/Documentation/Introduction>.
- [19] O. Chubar, P. Elleaume, and J. Chavanne, *J. Synchrotron Rad.* **5**, 481-484 (1998).
- [20] Frédéric Sirois, Mouhamadou Dione, François Roy, Francesco Grilli, Bertrand Dutoit, *Journal of Physics: Conference Series* **97**, 012030 (2008).
- [21] Kohei Higashikawa, Taketsune Nakamura, and Hiroshi Okamoto, *Supercond. Sci. Technol.* **18** 1445-1453 (2005).

- [22] S. Lee, W. S. Kim, S. H. Park, J. K. Lee, C. Park, J. H. Bae, K. C. Seong, H. Lee, J. H. Lee, K. Choi, and S. Hahn, IEEE Trans. Appl. Supercond. **20**, 1324-1328 (2011).
- [23] One should note that the elimination of stray fields requires some 3 or 4 times as much superconductor as would be possible in a solenoid, so there are significant cost considerations, in addition to stray field guidelines.
- [24] Our definition of  $J_c$  is essentially the engineering current density,  $J_c^{eng}$ , which is the critical current density scaled by the overall thickness of the conductor (*i.e.*,  $J_c \cdot (\text{Superconducting Layer Thickness})/(\text{Total Conductor Thickness})$ ).
- [25] We use *Radia* convenient units throughout the simulation, *i.e.*, all dimensions, fields and energies are given in millimeters, Tesla and Joules, and therefore we only use *Radia* units throughout the simulation and discussion.
- [26] G. Z. Li, Y. Yang, M. A. Susner, M. D. Sumption, and E. W. Collings, Supercond. Sci. Technol. **25**, 025001 (2012).
- [27] For the purposes of the MgB<sub>2</sub>-based SMES calculation, we have extracted the dimensions of the MgB<sub>2</sub> wire from the Scanning Electron Micrograph from Li *et al.* [26]. We take the outer radii of the Mg, MgB<sub>2</sub>, Nb and monel layers to be 0.1 mm, 0.146 mm, 0.325 mm and 0.417 mm, respectively, with a 50  $\mu\text{m}$  kapton sheath on the outside (total monocore thickness = 0.933 mm). The Mg, MgB<sub>2</sub>, Nb and monel densities are taken to be  $1.738 \times 10^{-3} \text{ g/mm}^3$ ,  $2.62 \times 10^{-3} \text{ g/mm}^3$ ,  $8.57 \times 10^{-3} \text{ g/mm}^3$  and  $8.857 \times 10^{-3} \text{ g/mm}^3$ , respectively. The critical current density,  $J_c(B)$ , is extracted from the data published by Li *et al.* [26].
- [28] A. P. Malozemoff, S. Fleshler, M. Rupich, C. Thieme, X. Li, W. Zhang, A. Otto, J. Maguire, D. Folts, J. Yuan, H.-P. Kraemer, W. Schmidt, M. Wohlfart, and H.-W. Neumueller, Supercond. Sci. Technol. **21**, 034005 (2008).
- [29] A. P. Malozemoff, Annu. Rev. Mater. Res. **42**, 373 (2012).
- [30] Martin W. Rupich, Xiaoping Li, Cees Thieme, Srivatsan Sathyamurthy, Steven Fleshler, David Tucker, Elliot Thompson, Jeff Schreiber, Joseph Lynch, David Buczek, Ken DeMoranville, James Inch, Paul Cedrone and James Slack, Supercond. Sci. Technol. **23**, 014015 (2010).
- [31] For the purposes of the YBCO-based SMES calculation we take that the YBCO tape comprises a 2  $\mu\text{m}$  YBCO, 50  $\mu\text{m}$  copper, 45  $\mu\text{m}$  stainless steel and 50  $\mu\text{m}$  kapton layers, respectively (see Section 3.3). We take the tape width to be 12 mm, and the densities of YBCO, copper, stainless steel and kapton to be  $6.3 \times 10^{-3} \text{ g/mm}^3$ ,  $8.92 \times 10^{-3} \text{ g/mm}^3$ ,  $8.03 \times 10^{-3} \text{ g/mm}^3$  and  $1.42 \times 10^{-6} \text{ g/mm}^3$ , respectively.
- [32] I. I. Mazin, Nature **464**, 183 (2010).
- [33] A. Gurevich, Phys. Rev. B **82**, 184504 (2010).
- [34] I. K. Dimitrov, W. D. Si, W. Ku, S. J. Han, and J. Jaroszynski, Low Temp. Phys. **39**, 680 (2013).
- [35] Z.-H. Liu, P. Richard, N. Xu, G. Xu, Y. Li, X. C. Fang, L. L. Jia, G. F. Chen, D. M. Wang, J. B. He, T. Qian, J. P. Hu, H. Ding, and S. C. Wang, Phys. Rev. Lett. **109**, 037003 (2012).
- [36] W. Si, J. Zhou, Q. Jie, I. Dimitrov, V. Solovyov, P. D. Johnson, J. Jaroszynski, V. Matias, C. Sheehan, and Q. Li, Appl. Phys. Lett. **98**, 262509 (2011).
- [37] W. Si, S. Han, X. Shi, S. N. Ehrlich, J. Jaroszynski, A. Goya, and Q. Li, Nature Commun. **4**:1347 doi: 10.1038/ncomms2337 (2013).
- [38] A. Xu, J. Jaroszynski, F. Kametani, Z. Chen, D. C. Larbalestier, Y. L. Viouchkov, Y. Chen, Y. Xie, and V. Selvamanickam, Supercond. Sci. Technol. **23**, 014003 (2010).
- [39] V. Braccini, A. Xu, J. Jaroszynski, Y. Xin, D. C. Larbalestier, Y. Chen, G. Carota, J. Dackow, I. Kesgin, Y. Yao, A. Guevara, T. Shi, and V. Selvamanickam, Supercond. Sci. Technol. **24**, 035001 (2011).
- [40] Nikolai Schwerg, Ph.D. thesis, Technical University of Berlin (2005).
- [41] For both simulations  $CR$  was increased from  $CR_0 = 400 \text{ mm}$  to its final value,  $CR = 700 \text{ mm}$ , in steps of 2 mm. The coil widths for the 2G and MgB<sub>2</sub>-based devices, however, were varied differently, since in the former case the natural step size the thickness of the tape (12 mm) while in the latter case, it is the thickness of the monocore strand. Therefore, for the YBCO-based SMES,  $W$  was varied in steps of 12 mm, while in the MgB<sub>2</sub> case, we arbitrarily picked the step size to be  $12 \times 0.933 \text{ mm}$  (monocore thickness = 0.933 mm). Larger coil radii and widths were purposely omitted from the simulation, since we noticed that at larger values of those, the coils would start to physically "overlap", leading to unphysical solutions.
- [42] The energy settings were subject to small changes, subordinating a stringent energy requirement to the objective of creating an optimized (70% load factor) SMES.
- [43] "Optimization" in this context could be defined to mean either the *i*) maximization of current-carrying capacity, or *ii*) the minimization of weight.